Temporal and Spatial Characterisation of Sea Ice Deformation

J.K. Hutchings, A. Roberts, C.A. Geiger, J.A. Richter-Menge, M. Thomas & C. Kambhamettu

Our Motivation: To identify an empirical stress strain-rate relationship, based on observational data, for pack ice at geophysical scales (10-1000 km).

Key Finding: Coherence of sea ice deformation over synoptic and larger scales is an emergent property of the forcing on the system. Deformation at sub-synoptic scales is not predictable from large scale observations, but does display fractal scaling.

The SEDNA Field Experiment

We investigate sea ice deformation observed with GPS-instrumented ice drifting buoys, and stress gauges, deployed during late winter through summer in the Beaufort Sea. The Sea Ice Experiment: Dynamic Nature of the Arctic (SEDNA) was designed to investigate the relationship between strain-rate, stress and thickness redistribution of Arctic pack ice. Here we focus on one of the four objectives of SEDNA: "Characterize the relationship between, and coherence of, stress and strain rate at 10km and 100km". Two nested arrays of six GPS buoys each (fig. 1), which were deployed in late March 2007 served as a backbone for the experiment. The two arrays were hexagons with initial widths of 140km and 20km.

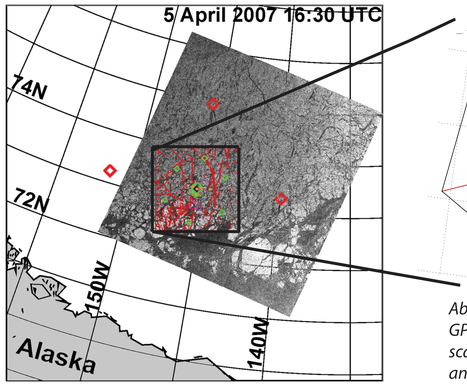

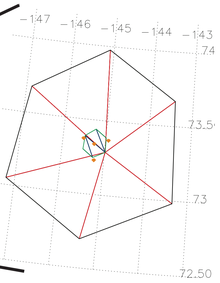

Figure 1: Site of SEDNA field experiment. Squares are buoy locations when the SAR image was acquired: red - met buoys, green - GPS, black - met station and IMB, orange - stress gauges. Red lines in the left panel are discontinuities in the velocity field, from analysis of two SAR images 2 days apart.

Above shows buoy arrays used in our scaling analysis. 12 GPS buoys are arranged into 4 sets of arrays, with length scales of around 10km (blue), 20km (green), 70km (red) and 140km (black).

Between March 26 and June 22 all 12 GPS buoys reported 10 minute positions. Position data was interpolated to hourly intervals. This is the maximum temporal resolution we can achieve, at 10 km scale, where GPS noise does not swamp strain-rate estimates (Hutchings et al. 2010). Strain-rate was calculated as Hutchings & Hibler (2008), Hutchings et al. (2010). The components of strain-rate (divergence, ε_I, and maximum shear, ε_{II}) are estimated for each buoy array in fig. 1 (fig. 2). We use the total deformation rate, $D=(\varepsilon_I^2+\varepsilon_{II}^2)^{1/2}$, in our scaling analysis.

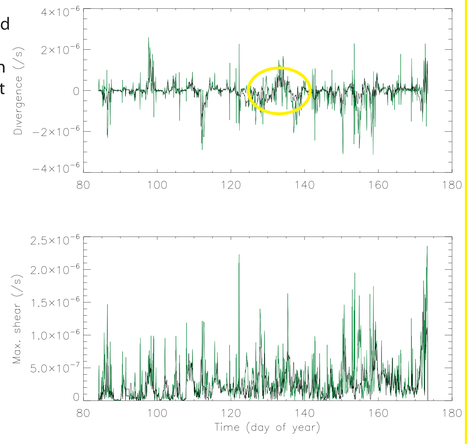

Figure 2: Time series of divergence and maximum shear for 140km (black) and 20km (green) wide hexagon buoy arrays. Strain rate components are also estimated for 70km (red) and 10km (blue) arrays, but are not shown here.
The circled period of opening occurred under a high pressure trough weather system in the Beaufort. Some degree of correlation between strain-rate at 20km and 140km was lost during this weather event.

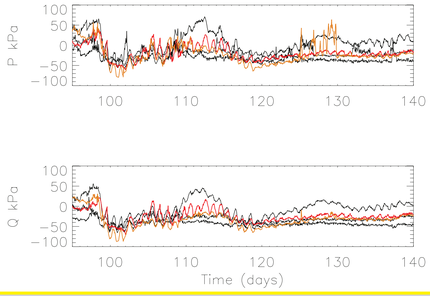

Figure 3: Invariants of internal ice stress (P & Q), measured by stress gauges. Each gauge measures stress experienced at a 'point'. This stress is a super-position of thermal and dynamic stress on the ice floe, and is related to the position of the stress gauge in the ice floe. By floe we are referring to the continuous connected ice between leads or ridges. Thermal stress has a clear diurnal cycle, and may have a synoptic component. Dynamic loading on the ice pack varies on synoptic scales. Failure events should have characteristic 'saw tooth' shape, as stress drops quickly after slow loading. Three gauges were deployed 10km from camp (black), one in FY ice near camp (orange), and one in MY ice near camp (red). Method to calculate P & Q is outlined by Cox & Johnson (1983).

First, we investigate scaling of sea ice deformation using similar techniques to Marsan et al. (2004) (fig.4) and Rampal et al. (2009) (fig. 5). From the buoy array hourly deformation time series (fig. 2) , we find the mean and variance at the four scales identified in fig. 1. Time scaling is investigated by sub-sampling each deformation time series at 10 minute - 10 day periods. We perform this for each sub-array.

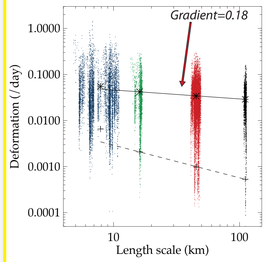

Figure 4: Deformation (mean: stars, variance: crosses) demonstrates log-log scaling with length scale, across 2 orders magnitude in scale. The exponent H=0.18, is the same as that Marsan et al. (2004) found.

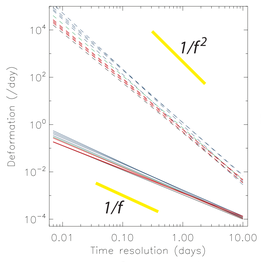

Figure 5: Deformation (mean: solid lines, variance: dashed lines) demonstrates scaling with time scale. The mean and variance have differing scaling relations, demonstrating multi-fractalility.

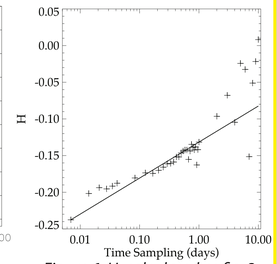

Figure 6: H, calculated as fig. 3, for different time sampling periods. The gradient of the least squares fit is 0.5 /day, varies by +/- 0.1 /day when estimated over smaller intervals.

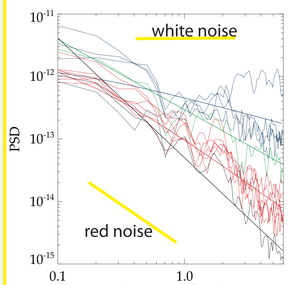

Figure 7: Fourier transform of divergence time series (as fig. 2), for each sub-array. Colors as fig. 1.

- Spatial and temporal scaling is coupled (as Rampal et al. 2009).
- Hence we can estimate spatial scaling from spectral analysis of time series.
- Deformation is a 'pink noise' process. 'Whitening' indicates greater dissipation in ridges. The forcing (winds, ocean currents) have red noise character, and in the absence of dissipative energy losses, we could expect deformation to show 'red noise' character.
- Dissipation is greater at smaller scales, consistent with localization of strain-rate at leads/ridges.
- Deformation variance increases at smaller scales, and spectra 'whitens', consistent with reducing coherence as smaller scales. Suggesting dissipative processes 'win over' force balance, locally.
- At 140km scale, deformation is close to 'red noise', indicating it is primarily driven by synoptic activity at this scale.
- Deformation is multi-fractal. If it were mono-fractal we would expect fig. 7 and fig.5-mean to show same scaling. They do not.
- This means variance, and higher statistical moments, are needed to describe scaling properties of sea ice deformation.

Observation scale impact on ice growth estimates

Given a time series of divergence, we can model the growth of ice in leads and ridging of this ice. Our model (Hutchings & Rigor 2010) assumes Maykut & Untersteiner (1971) growth rates, and that thinnest ice is ridged preferentially. We estimate the total volume of ice grown in leads during the SEDNA experiment, for each buoy array divergence, calculated with hourly resolution, at length scales ranging from10-140km (fig. 8). This volume is normalized by array area to give mean new ice thickness in the array. We also consider the divergence calculated with varying time scale (10 minutes - 10 days), for each buoy array (fig. 9). The basal ice growth was about 20 cm for ice that was present when GPS buoys were deployed.

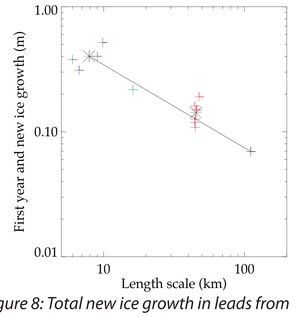

Figure 8: Total new ice growth in leads from March 26 to June 22 within each buoy array. The line is a least square fit to mean new ice thickness across arrays of similar scale (stars) on June 22. Gradient of the fit is ~7m/km.

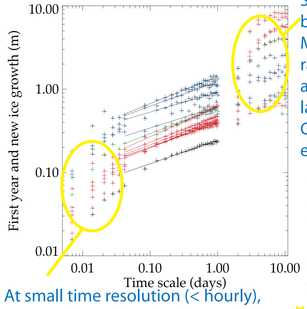

Scaling relation breaks down as M&U71 growth rates are not appropriate for large time steps. Growth is over-estimated on opening

Figure 9: Total new ice growth, estimated for each buoy array as fig. 8, using GPS position data with varying time sampling (time scale). We perform a least square fit for each buoy array over the time sampling range that is not significantly impacted by errors imparted by our methodology or measurements. These lines have gradient 0.30 m/day, with standard deviation 0.03m/day.

At small time resolution (< hourly), and small spatial scales (<4km), GPS noise swamps strain-rate estimates. Lower precision positioning (e.g. RGPS, ARGOS) have larger time and space scale cutoffs below which strain-rate estimates are meaningless.

- We show that below the synoptic scale the scale of deformation observation (or model) is important in the sea ice mass balance.
- If lead scale, with hourly GPS resolution, position data is not available: improve accuracy of seasonally integral parameters (e.g. ice growth, total heat flux to atmosphere) with a fractal model for ice deformation below grid scale.

Is there a deformation de-correlation length scale?

We performed wavelet cross-coherence analysis between divergence of the 20 km and 140 km arrays, using the methods of Grinsted et al. (2004). This indicates the level of coherence between the two signals energy densities for all periods represented in the time series.

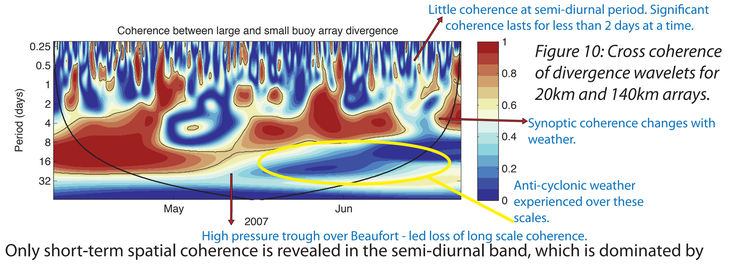

Figure 10: Cross coherence of divergence wavelets for 20km and 140km arrays.

Only short-term spatial coherence is revealed in the semi-diurnal band, which is dominated by inertial, rather than tidal, oscillations. Additional wavelet analysis (not shown) suggests that during periods of increased cyclonic (anti-cyclonic) weather deformation on the large (small) scale leads the small (large) scale. Coherence over longer scales, during cyclonic periods, is consistent with reddening of the system, and transfer of stress information over longer scales.

- External forcing (wind) is driving the system at larger scales to a red process (memory across L/T).
- Coherent deformation at synoptic time scales and larger is an emergent property of the forcing on the system.
- At smaller scales, increased deformation variance whitens the process. This is driven by damping through ice interaction, and causes information (stress) disconnection over smaller scales.

Answer: NO!

How to relate observed stress to strain-rate? Future Direction

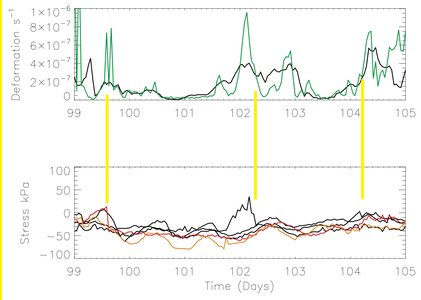

Figure 11: Part of deformation (top) and total stress, $(P^2+Q^2)^{1/2}$ (bottom), time series. Three fracture events are indicated with yellow lines. These are identified where stress drops rapidly. Note deformation rate increases after each fracture event.

There is no clear coherence between stress and deformation. Fracture events are only observed in single stress time series. This suggests stress at fracture is heterogeneous over less than 10km scales. We expect fracture stress to be a random, white noise, process.

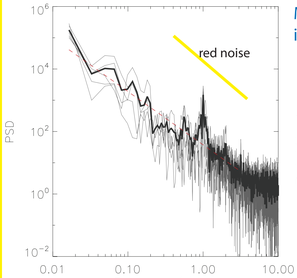

Figure 12: Fourier spectra of total stress for stress gauges (grey). Dashed line is fit to mean spectrum (black). Gradient of fit is -1.7. Suggesting much of signal is linearly related to forcing (weather).

Most power in stress time series is related to the diurnal cycle, in thermal stress, and weather (fig. 12).

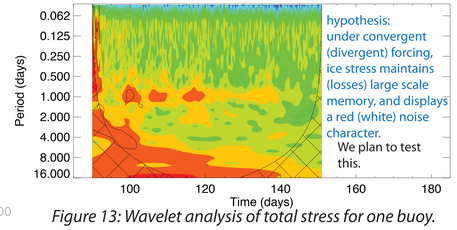

Figure 13: Wavelet analysis of total stress for one buoy. Note spectra whitens after day 130, and diurnal cycle reduces. This is common across all buoys. Is this related to synoptic changes and/or progression of spring, when ice pack becomes less 'connected'?

Does this mean stress dissipation due to deformation is small? We expect not - as it is significant in the ice pack force balance (Hunkins 1975).

The strain-rate scaling analysis demonstrates local strain-rate cannot be predicted from a regional measurement. Stress at a point in the ice pack is related to confining stress (wind, current, geometry) which controls fracture spacing, and the distance to leads (where normal stress to lead is zero) and ridges (where stress is dissipated). Numerical modelling could allow us to determine how the stress field, and time series of stress at a point, is related to ice strength (thickness/age) distribution, fracture spacing and confining stress in the vicinity of the point. Mapping of deformation features (by VIMS lab) will allow us to relate distance from measurement point to fracture, and fracture spacing. Such that we can investigate length scale over which stress relaxation due to failure is felt. Our working hypothesis is that this is the fracture spacing, as our strain-rate analysis indicates information transfer at this scale is minimal. However, fig 13. suggests the loading stress (likely a red process) is important over long scales in a converging ice pack - echoing the interpretation of fig. 10.

References

(1) Cox, G. F. N. and J. B. Johnson, 1983. Stress measurements in ice, CRREL Report 83-23. (2) Grinsted, A., J. C. Moore and S. Jevrejeva, 2004. Application of the cross wavelet transform and wavelet coherence to geophysical time series, Nonlinear Processes in Geophys., 11, 561–566. (3) Hunkins, K., 1975. "The ocean boundary layer and stress beneath a drifting ice floe", JGR, 80(24), 3425–3433. (4) Hutchings, J. K., P. Heil, A. Steer and W. D. Hibler III, 2010. Sub-synoptic scale spatial variability of sea ice deformation in the western Weddell Sea during early summer., submitted to J. Phys. Oceanogr. (5) Hutchings, J. K. and W. D. Hibler III, 2008. Small-scale sea ice deformation in the Beaufort Sea seasonal ice zone, J. Geophys. Res.,113, doi:10.1029/2006JC003971. (6) Hutchings, J. K. and I. G. Rigor, 2010. Trends in Beaufort Sea Ice Pack Deformation, in preperation for GRL. (7) Marsan, D., H. Stern, R. Lindsay and J. Weiss, 2004. Scale dependence and localization of the deformation o f Arctic sea ice, Phys. Rev. Lett., 93(17), 178501. (8) Maykut, G. A. and N. Untersteiner, 1971. Some results from a time-dependent thermodynamic model of sea ice, J. Geophys. Res., (9) Rampal, P., J. Weiss, D. Marsan, R. Linday and H. Stern, 2008. Scaling properties of sea ice deformation from buoy dispersion analysis, J. Geophys. Res., 113, doi:10.1029/2007JC004143.

Acknowledgements

Funding for this project has been provided by grant 0612527 from the National Science Foundation, Office of Polar Programs. We wish to express our deep gratitude to Fred Karig and his team from the Applied Physics Laboratory who directly supported our work in the field. This experiment would not have occurred without the support of Jeff Gosset, the Arctic Submarine Laboratory and the US Navy. We particularly thank Pat Mckeown, "Andy" Anderson and Randy Ray who deployed our GPS ice drifters. NCEP-NCAR reanalysis products were used in our interpretation of fig 10.. Hutchings thanks David Newman and participants of the 2010 Complex Systems Workshop, held at UAF March 8-11, for insightful discussions. Any opinions, findings, and conclusions or recommendations expressed in this material are those of the authors and do not necessarily reflect the views of the National Science Foundation.